(Preprint) AAS 25-675

LOCAL ORBITAL ELEMENTS WITH HALO ORBITS

Luke T. Peterson,[*] Ethan Dennis,[†] and Daniel J. Scheeres[‡]

Cislunar local orbital elements (LOEs) can simplify the form of dynamics around Lagrange points in the Earth-Moon circular restricted 3-body problem, and have many uses: tracking cislunar trajectories, rapidly predict natural dynamics, stationkeeping orbits. However, the primary limitation of LOEs is the exclusion of halo and quasi-halo orbits; hence, resonant local orbital elements (RLOEs) have been developed to re-incorporate these orbits into the LOE framework. In this work, we review the relevant resonant normal form theory used to construct RLOEs. Using RLOEs, orbits can be readily generated from Poincaré sections; conversely, one can utilize the same Poincaré sections to track arbitrary trajectories within a substantial region around the Lagrange points, and relate arbitrary trajectories to Lagrange point orbits. In this article, we show an example of RLOEs as a Strategic Visualization Tool. Further, we show that the Flow Map Parameterization Method (FMP) for computing quasi-periodic orbits enables a similar and effective generalization of the Floquet mode approach for stationkeeping quasi-halo orbits. We compute a quasi-halo orbit using FMP, and perform a posteriori analysis using the RLOE Strategic Visualization Tool. Finally, we propose a simulation to generate a controlled spacecraft trajectory using the Floquet mode approach for stationkeeping, and discuss how the RLOE Strategic Visualization Tool may be applied.

INTRODUCTION

Understanding the dynamics in cislunar space has become increasingly important with the announcement of the Lunar Gateway and the Artemis program.[1,2] Around the Lagrange points in cislunar space, the gravitational forces of the Earth and Moon are of similar magnitudes and neither can be neglected. Due to the presence of multiple significant gravitational forces, we model the dynamics of a spacecraft in these regions using a 3-body problem rather than a 2-body problem. In particular, we use the circular restricted 3-body problem (CR3BP) as a simplified model accurately capturing cislunar dynamics. While one can use 2-body orbital elements, e.g., Keplerian orbital elements, to understand dynamics in a geometric coordinate set in the 2-body setting with perturbations, the perturbing force of the Earth or Moon near the Lagrange points is too great for these elements to provide useful information.[3] To combat this, local orbital elements (LOEs) have been developed to provide a similar set of geometric coordinates that simplify the form of the dynamics near the Lagrange points.[4] As the CR3BP is not integrable, LOEs are only defined locally around a particular Lagrange point. Due to the transformations required to simplify the form the dynamics near Lagrange points in the derivation of LOEs, the resonant terms in the Hamiltonian function describing the spacecraft's motion are removed, and the halo orbits are consequently lost. So, how important are the halo orbits, and how can we re-incorporate them into our LOE framework?

[*]Postdoctoral Researcher, Aerospace Engineering Sciences, University of Colorado, Boulder, Colorado 80309, USA.
[†]Ph.D. Student, Aerospace Engineering Sciences, University of Colorado, Boulder, Colorado 80309, USA.
[‡]Distinguished Professor, A. Richard Seebass Chair, Aerospace Engineering Sciences, University of Colorado, Boulder, Colorado 80309, USA.

The Lunar Gateway has been proposed to fly on a southern halo orbit about EM L_2; hence, additional halo and quasi-halo orbits are likely to be used for staging orbits near gateway, making their use more prominent.[1] In order to increase the impact of local orbital elements in cislunar space, we seek to incorporate halo orbits into the existing framework. The LOEs are constructed by putting the CR3BP Hamiltonian function around a Lagrange point into an integrable normal form, i.e., by constructing three constants of motion around $L_{1,2}$ through a series of canonical transformations. By altering the form of the canonical transformations, we can retain resonant terms, thus keeping the halo and quasi-halo orbits, at the expense of one constant (integral) of motion. In other words, to keep the halo orbits we can have only two integrals–one for the saddle (hyperbolic motion), one for a single center (oscillatory motion). Following the clever work done by Celletti,[5] Pucacco,[6] and Paez,[7] we creatively construct action-angle variables which parameterize both the periodic and quasi-periodic orbits in the region: planar and vertical Lyapunov, Lissajous, halo, and quasi-halo. In this way, the local orbital element framework is modified to incorporate halo orbits via so-called resonant local orbital elements (RLOEs). This work recapitulates and expands upon the description in Peterson and Scheeres (2024).[8] In particular, RLOEs enable the construction of Strategic Visualization Tool; in effect, the RLOE representation provides an effective and intuitive vector space decomposition into center and saddle projections. Similar to the 2-body orbital elements, in which one can associate an arbitrary position and velocity to a corresponding orbit, the Strategic Visualization Tool offers the same insight in the vicinity of the Lagrange points, where the corresponding orbits can be periodic orbits, quasi-periodic orbits, or generic saddle trajectories.

The visualization tool is useful for identifying nearby orbits and unstable components along trajectories; hence, stationkeeping offers a natural application of the tool. In the (R)LOE decomposition, Peterson and Scheeres[4] described a technique for stationkeeping that eliminates the unstable coordinate, q_1, in the normal form. This strategy was applied by Hunsberger et al. (2025)[9] using both LOEs and RLOEs via Birkhoff and resonant normal forms, respectively. There are trade-offs to use normal form methods; more often than not, the trade-off is accuracy for simplicity. Performing stationkeeping maneuvers in the normal form (LOE/RLOE) representation, one loses accuracy in the underlying dynamics, but the simplicity is lost, as a Newton method is required for obtaining a suitable ΔV to nullify the unstable coordinate. Especially, as accuracy has a higher importance in stationkeeping calculations, if there is no significant ease in maneuver description, can we avoid the trade-off and the normal form altogether? If so, is there a morally similar stationkeeping approach that utilizes the geometry of the nominal orbit? The strategy we seek is the Floquet mode approach.

The Floquet mode approach is a control strategy to nullify the unstable component of the normal direction for a nominal orbit. Developed originally by Wiesel and Shelton[10] for periodic orbits, Simó et al. (1986)[11] describe the possibility of applying the technique to quasi-periodic orbits. In first of their four seminal books, Gomez et al. (2001)[12] detail the construction of the Floquet modes using the nominal orbit's monodromy matrix–while this was done previously, the detail is worth noting for a reader looking to implement the method. The Floquet mode approach has been compared with other stationkeeping techniques, such as the target point approach,[13] principal stretching directions (PSDC) and phase augmented crossing control (PACCMAN).[14] Farres et al. (2022)[15] analyze the geometry of two stationkeeping strategies, Floquet mode control and the velocity constraint approach, finding that both methods successfully cancel the unstable mode. Zhou et al. (2021)[16] later implement a Floquet mode-like approach for quasi-periodic Lissajous orbits, not depending on the variational equations but rather relying on a covariance-based orbit maintenance controller. Using the Flow Map Parameterization method,[17] the orbit and its tangent and normal directions are computed simultaneously, and these directions can be readily modified to produce the Floquet basis on which the Floquet mode approach is built. Hence, we compute a quasi-halo orbit around EM L_1 in the CR3BP using FMP, and we derive the Floquet modes for quasi-periodic orbits in the CR3BP. Additionally, we comment on generalizing the approach for quasi-periodic orbits in periodically-perturbed models of cislunar space (e.g., ER3BP and R4BPs).

This paper reintroduces resonant local orbital elements (RLOEs) with several new applications to spaceflight mechanics and will be organized as follows. First, we derive the resonant normal form for the Earth-Moon CR3BP around $L_{1,2}$. We exploit the two integrals that are constructed in the resonant normal form in order to define an region of validity around $L_{1,2}$ and includes halo and quasi-halo orbits. We demonstrate results around Earth-Moon $L_{1,2}$, parameterizing Lyapunov and halo periodic orbits as well as Lissajous and quasi-halo quasi-periodic orbits. We generalize the visualization techniques from the original LOEs into RLOEs, packaging them into the so-called RLOE Strategic Visualization Tool. Next, we describe the Flow Map Parameterization method for computing quasi-periodic orbits and compute a quasi-halo orbit. Then, we generalize the Floquet mode approach for stationkeeping from periodic to quasi-periodic Lagrange point orbits, following a similar philosophy of strategies previously developed for LOEs. Finally, we propose a simulation and describe how the RLOE Strategic Visualization Tool can be used for a posteriori analysis.

RESONANT LOCAL ORBITAL ELEMENTS

In this work, we modify the existing framework of local action-angle orbital elements in the CR3BP to include halo and quasi-halo orbits, due to their utility in the preliminary mission design process. In order to incorporate halo orbits, we must ensure the resonant terms which were removed during the construction of the Birkhoff normal form are not removed. We will recover the halo orbits at the cost of one formal integral in the center manifold; however, the global energy integral of the system will allow the system to be approximately integrable in the now larger region where the local orbital elements well approximate the dynamics of the original system.

Normal Form Theory

Local orbital elements are a set of coordinates in the CR3BP following a set of normalizing transformations about a bounded invariant manifold, e.g., consider EM L_1 and L_2 in the present work. Defining conjugate momenta as $p_x = \dot{x} - y$, $p_y = \dot{y} + x$, and $p_z = \dot{z}$, the CR3BP equations of motion can be written in Hamiltonian form, with Hamiltonian function given by[3]

$$H = \frac{1}{2}\left(p_x^2 + p_y^2 + p_z^2\right) + yp_x - xp_y - \frac{1-\mu}{r_1} - \frac{\mu}{r_2}, \tag{1}$$

where r_1 is the distance from the larger primary, and r_2 is the distance from the smaller primary. We recenter and scale these coordinates around $L_{1,2}$:

$$X = -\gamma_j x + \mu + a, \quad Y = -\gamma_j y, \quad Z = \gamma_j z, \tag{2}$$

where γ_j is the distance between L_j and the nearest singularity, e.g., the smaller primary, and where $a = -1 + \gamma_1$ for L_1 and $a = -1 - \gamma_2$ for L_2.

Next, we write the re-centered and scaled Hamiltonian function as an infinite series using the Richardson expansion.[18] In short, expand the dipole terms of H, $\frac{1-\mu}{r_1}$ and $\frac{\mu}{r_2}$, using the dipole expansion:

$$\frac{1}{\sqrt{(x-A)^2+(y-B)^2+(z-C)^2}}=\frac{1}{D}\sum_{n=0}^{\infty}\left(\frac{\rho}{D}\right)^n P_n\left(\frac{Ax+By+Cz}{D\rho}\right), \tag{3}$$

where $D^2=A^2+B^2+C^2$, $\rho^2=x^2+y^2+z^2$, and P_n is the Legendre polynomial of degree n. Using the above expansion, we obtain the original Hamiltonian now re-centered about an equilibrium point and written as an infinite series:

$$H=\frac{1}{2}(p_x^2+p_y^2+p_z^2)+yp_x-xp_y-\sum_{n\geq 2}c_n(\mu)\rho^n P_n\left(\frac{x}{\rho}\right), \tag{4}$$

where the $c_n(\mu)$ are real coefficients depending on μ and γ_j.

Taking the Hamiltonian in Equation 4, we apply a linear symplectic change of variables putting the quadratic terms into their real normal form:

$$H_2=\lambda xp_x+\frac{\omega_1}{2}(y^2+p_y^2)+\frac{\omega_2}{2}(z^2+p_z^2), \tag{5}$$

where the coefficients depend on the choice of system, i.e., μ, and the equilibrium point, i.e., L_1 or L_2. Note that the linear system H_2 is integrable with three integrals:

$$I_1=xp_x,\quad I_2=\frac{1}{2}(y^2+p_y^2),\quad I_3=\frac{1}{2}(z^2+p_z^2), \tag{6}$$

so we can write $H_2=H_2(I)$.

In practice, we change to complex variables for ease of computation wherein the Hamiltonian takes the form:

$$H=\lambda xp_x+\mathtt{i}\omega_1 yp_y+\mathtt{i}\omega_2 zp_z+\sum_{n\geq 3}H_n(q,p), \tag{7}$$

where $\mathtt{i}=\sqrt{-1}$. By complexifying the terms corresponding to the linear center directions, we make uniform the integrals of motion that we wish to maintain: $I_j=q_jp_j$. We call the coordinates following this set of transformations the “diagonal” coordinates.

Once the Hamiltonian is in the form of Equation 7, we apply the Lie series method to construct symplectic changes of variables preserving the integrability of the transformed Hamiltonian at each order. The transformed Hamiltonian after a transformation generated by a function G is:

$$\hat{H}=H+\{H,G\}+\frac{1}{2!}\{\{H,G\},G\}+\cdots+\frac{1}{n!}L_G^n(H)+\cdots, \tag{8}$$

where $L_G^n(H)$ is the n-th Lie derivative of H generated by G, i.e., the n-fold nested Poisson bracket with G. The function G is determined at each order based on the desired style of normal form. In the original formulation of local orbital elements, we put the Hamiltonian into a Birkhoff (or integrable) normal form so that local integrability is preserved. As an example, consider the transformation G_3 to realize the third-order terms H_3 into a Birkhoff normal form. To put the terms H_3 into a Birkhoff normal form means to remove all terms:

$$\hat{H}_3=0=H_3+\{H_2,G_3\}, \tag{9}$$

where H_2 and H_3 are known. We solve this homological equation for G_3 explicitly:

$$G_3(q,p) = \sum_{|k_q|+|k_p|=3} \frac{-h_{k_q,k_p}}{\mathtt{i}\langle k_p - k_q, \omega\rangle} q^{k_q} p^{k_p}, \tag{10}$$

where we use the multi-indices k_q and k_p, $H_n = \sum_{|k_q|+|k_p|=n} h_{k_q,k_p} q^{k_q} p^{k_p}$, and ω is the linear frequency vector corresponding to the equilibrium point: $\omega = (\lambda, \omega_1, \omega_2)$. Repeating this process at odd degrees is the same, however, for even degrees, there are non-removable terms of the form: $k_q = k_p$. Thus, an equivalent approach to constructing a normal form of a particular style is to condition the multi-indices (k_q, k_p) for conditions under which to keep terms of a predetermined form. For example, imposing the condition $k_q = k_p$ generates a Birkhoff normal form. To construct a 1:1 resonant normal form, i.e., the normal form used to construct RLOEs, around a collinear Lagrange point, these conditions are:

$$k_{q_1} = k_{p_1}, \quad (k_{q_2} - k_{p_2}) + (k_{q_3} - k_{p_3}) = 0, \tag{11}$$

where (q_1, p_1) denote the saddle coordinates, and (q_2, p_2, q_3, p_3) denote the center coordinates.

Following the normalizing transformations putting H into its 1:1 resonant normal form up to degree N, the resulting Hamiltonian has the form:

$$H_N(q_1 p_1, q_2, p_2, q_3, p_3) = H_N(I_1, q_2, p_2, q_3, p_3), \tag{12}$$

where $I_1 = q_1 p_1$ is the saddle integral constructed by the first multi-index condition. In the Birkhoff normal form, recall that we defined action-angle variables in the variables (q_2, p_2, q_3, p_3) corresponding to the center manifold:

$$I_2 = \frac{1}{2}(q_2^2 + p_2^2), \quad \theta_2 = \arctan(p_2/q_2), \tag{13}$$

$$I_3 = \frac{1}{2}(q_3^2 + p_3^2), \quad \theta_3 = \arctan(p_3/q_3). \tag{14}$$

In the case of the Birkhoff normal form, I_2 and I_3 were first integrals by construction. For the 1:1 resonant normal form, while I_2 and I_3 are not first integrals, we can still apply this canonical change of variables to see that H_N takes the following form:

$$H_N(I_1, q_2, p_2, q_3, p_3) = H_N(I_1, I_2, I_3, \theta_2 - \theta_3). \tag{15}$$

In other words, the resonant normal form depends not only on the actions but also on resonant terms depending on the difference of the center angles corresponding to the 1:1 resonance. Thus, applying Hamilton's equations, we obtain:

$$\frac{d}{dt}(I_2 + I_3) = \frac{\partial H}{\partial \theta_2} + \frac{\partial H}{\partial \theta_3} = \frac{\partial H}{\partial \theta_2} - \frac{\partial H}{\partial \theta_2} = 0, \tag{16}$$

so that $I_2 + I_3$ is a first integral.

Note that one can obtain the so-called center manifold reduction by removing the second condition in Equation 11. By removing the second condition, the resulting Hamiltonian possesses only the saddle integral. The benefit is that the radius of validity is increased, similar to the increase in validity when going from Birkhoff to 1:1 normal form. The figure below shows a comparison between these three normal form styles via Poincaré sections of the center manifold. Note that the integrable (Birkhoff) normal form is concentric circles with no halo orbits; the resonant normal form contains the halo orbits and some of the symmetry of the integrable case; the center manifold reduction is the closest to the real picture of the dynamics around L_1. When exploiting normal form methods for astrodynamics, one must consider the trade-offs between accuracy and simplicity.

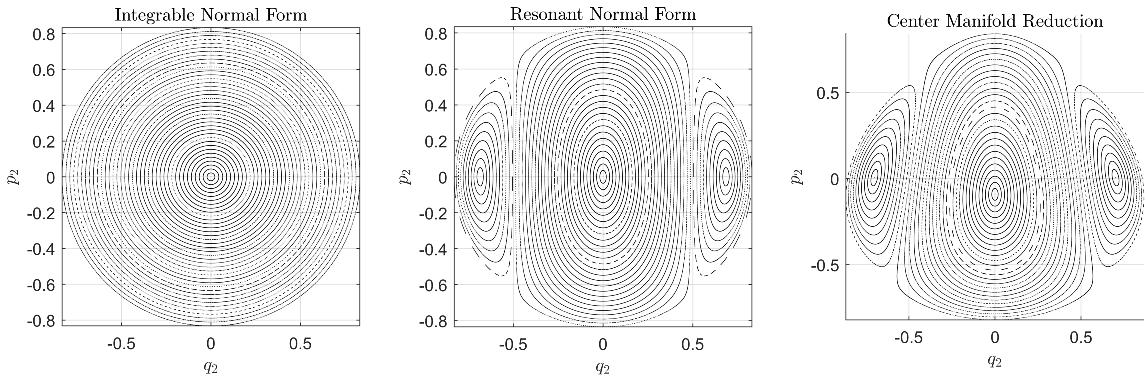

Figure 1. The effect of normal form style on the center manifold around EM L_1 with $h = 0.8$.

Resonant Local Orbital Elements

To define local orbital elements in the 1:1 resonant normal form, we will perform an additional symplectic transformation from the typical action-angle variables to exploit this additional first integral, $I_2 + I_3$, as well as the dependence of H on the difference in angles, $\theta_2 - \theta_3$. Let us follow Paez[7] and define the following canonical change of variables from the classical action-angle variables $(I_2, I_3, \theta_2, \theta_3)$ to the modified action-angle variables $(\hat{I}_2, \hat{I}_3, \hat{\theta}_2, \hat{\theta}_3)$:

$$\hat{I}_2 = I_2, \quad \hat{I}_3 = I_2 + I_3, \tag{17}$$

$$\hat{\theta}_2 = \theta_2 - \theta_3, \quad \hat{\theta}_3 = \theta_3. \tag{18}$$

As an abuse of notation, we will refer to the set of local orbital elements $(I_1, \theta_1, \hat{I}_2, \hat{\theta}_2, \hat{I}_3, \hat{\theta}_3)$ removing the $\hat{}$ symbol. In practice, we may replace the saddle coordinates (I_1, θ_1) with the normal form coordinates (q_1, p_1), as q_1 and p_1 correspond to the unstable and stable manifold coordinates, respectively. In particular, we will consider how well the Floquet mode approach for stationkeeping nullifies the coordinate q_1. In the following section, we will see how periodic Lyapunov and halo orbits, as well as quasi-periodic Lissajous and quasi-halo orbits, can be simply generated using the resonant local orbital elements in the 1:1 resonant normal form.

Orbit Generation via Poincaré Maps

The local orbital element framework allows for simple computation of periodic and quasi-periodic orbits in normal form dynamics which approximate the original system around a Lagrange point. For the Birkhoff normal form, the simplified system is integrable, and periodic and quasi-periodic orbits can be generated by specifying action variables and allowing the angular variables to vary in $[0, 2\pi)$. For the resonant normal form, the simplified system is no longer fully integrable. Rather, we have only one integral in the center manifold, I_3 by construction. Instead of choosing two actions and varying each angle, the starting point for generating orbits in the resonant normal form is to consider the Poincaré map of the center manifold in local orbital elements. Generating this map is simple to do in normal form coordinates (q_2, p_2) and transform into local orbital elements. From the Poincaré map, we need only choose an invariant curve by fixing a discretization of (I_2, θ_2) and varying $\theta_3 \in [0, 2\pi)$. Thus, to retain the halo and quasi-halo orbits via resonant normal form, generating periodic and quasi-periodic orbits is as simple as generating a Poincaré map and varying a single angle; moreover, once a Poincaré map is generated, many orbits can be easily generated at a given local energy level. Figures 3 show the resulting generation of Northern and Southern quasi-halo orbits along with a Lissajous orbit at a fixed local energy level around EM L_1.

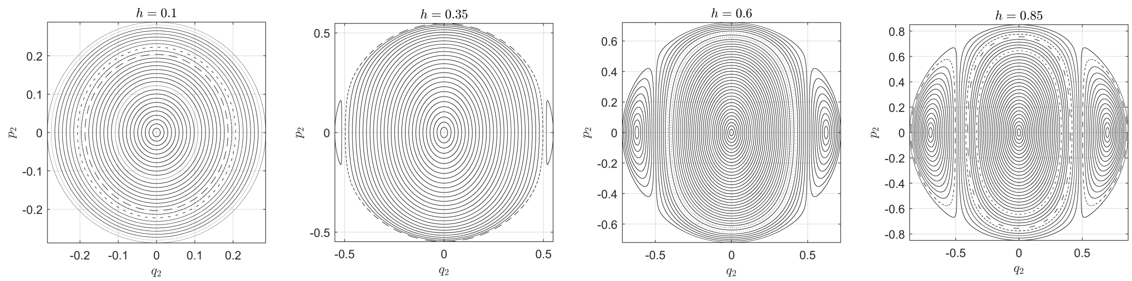

Figure 2. Poincaré section of the center manifold around EM L_1.

Strategic Visualization Tool

A primary benefit of the local orbital element framework is a random state around a Lagrange point, especially EM $L_{1,2}$, can be decomposed into an orbit and a saddle trajectory. For LOEs, this is reduced to transforming the spacecraft state into LOEs and projecting onto the center and saddle coordinates as subspaces. While the LOE decomposition is simple and intuitive for understanding libration point dynamics, the cost of removing halo and quasi-periodic orbits outweighs the benefit. So, in the present work, we take a similar approach using RLOEs; however, to visualize the underlying orbit, we must add to our analysis a visualization of a Poincaré section of the center manifold, rather than generating orbits directly from the LOE action-angle variables. This step turns out to be straightforward, and the visualization benefits remain now including halo orbits.

Consider a random point, $X_{\text{Cart}} = (x, y, z, \dot{x}, \dot{y}, \dot{z})$, around Earth-Moon L_1. Mapping X_{Cart} into RLOEs produces a point $X_{\text{RLOE}} = (q_1, p_1, I_2, \theta_2, I_3, \theta_3)$. To project onto the center subspace, in LOEs, the pair of action-angle variables are decoupled and so we can project onto pairwise coordinate subspaces, i.e., (I_2, θ_2) are the planar center coordinates and (I_3, θ_3) the vertical center coordinates. However, in RLOEs, the pair of action-angle variables are not decoupled. Hence, rather than projecting onto pairwise coordinate subspaces, we project onto the Poincaré section of the center manifold. Projecting onto the center manifold means setting $(q_1, p_1) = (0, 0)$. Projecting onto the Poincaré section of the center manifold requires shifting an angle to the one corresponding to the appropriate section. We project onto the Poincaré section by shifting $\theta_3 \to \pi/2$ by flowing along the center manifold for some time $t^* \in [-T/2, T/2]$: $\phi^{\text{CM}}_{t^*}(X_{\text{RLOE}})$, where T is the return time to the section. Note that one can choose $\theta_2 \to \pi/2$ to instead consider the vertical section. A shift in θ_3 (θ_2, respectively) requires an update to (I_2, θ_2) which can be obtained from the center manifold flow, i.e., $\phi_{t^*}^{\mathrm{CM}}(X_{\mathrm{RLOE}})$. Since I_3 is constant, one can imagine the Poincaré section of the center manifold sweeping multiple angles θ_3, the corresponding point will thus rotate around the invariant curve. The invariant curve stays the same, the angle θ_2 is corrected from the rotation number, and the action I_2 is found on the section as $I_2(\theta_2)$. The result is a quasi-periodic orbit (Lissajous or quasi-halo) that is related to the random point through RLOE projection. Note that the energy of the center manifold projection is likely different from the energy of the random point, since the saddle contributes to the energy away from the q_1 and p_1 axes.

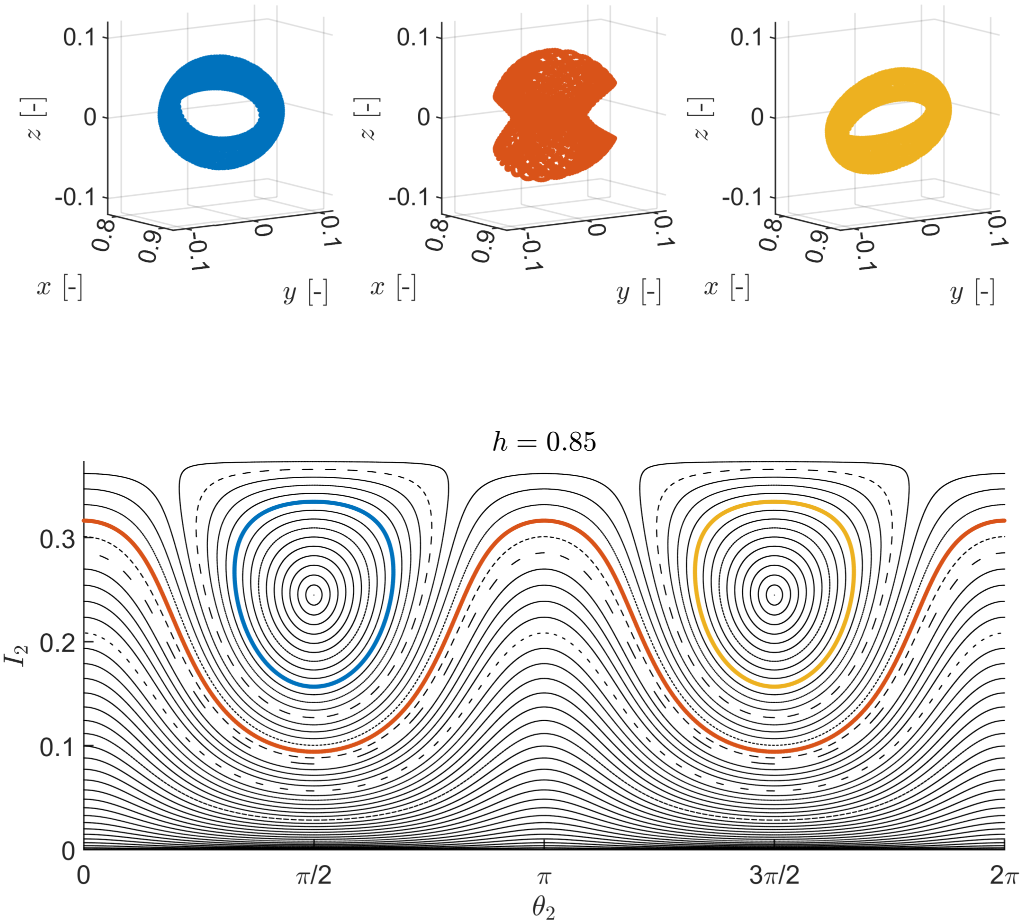

Figure 3. EM L_1 Quasi-halo and Lissajous orbits generated from RLOEs.

Projecting onto the saddle manifold is identical to the LOE case, i.e., as the center and saddle are decoupled, we project onto the saddle manifold by setting $(I_2, \theta_2, I_3, \theta_3) = (0, 0, 0, 0)$, or really $(q_2, p_2, q_3, p_3) = (0, 0, 0, 0)$ to avoid singularities of action-angle variables. The saddle projection tells us the hyperbolic and transiting behaviors of the random point's trajectory, as well as useful information for maneuvering onto the corresponding orbit generated from the center manifold projection. Indeed, the distance from the origin in the saddle plane is related to the magnitude of ΔV required to stabilize the trajectory onto the stable manifold of the nominal, or underlying, orbit using the Floquet mode approach for stationkeeping.

Figure 4 shows the RLOE decomposition described above for a random point around Earth-Moon L_1. Note that the saddle projection indicates the transiting behavior of the point, and the center projection identifies a Northern quasi-halo orbit corresponding to the random point. Repeating the above analysis for a random point around Earth-Moon L_2 yields Figure 5. Note that the saddle projection indicates non-transiting behavior, rather, the random trajectory stays on the side nearest the Moon. Further, the center projection identifies a Lissajous orbit corresponding to the random point. Observe in each case the random points ultimately lie on generic saddle trajectories, locally combinations of the stable and unstable manifolds of quasi-periodic libration point orbits.

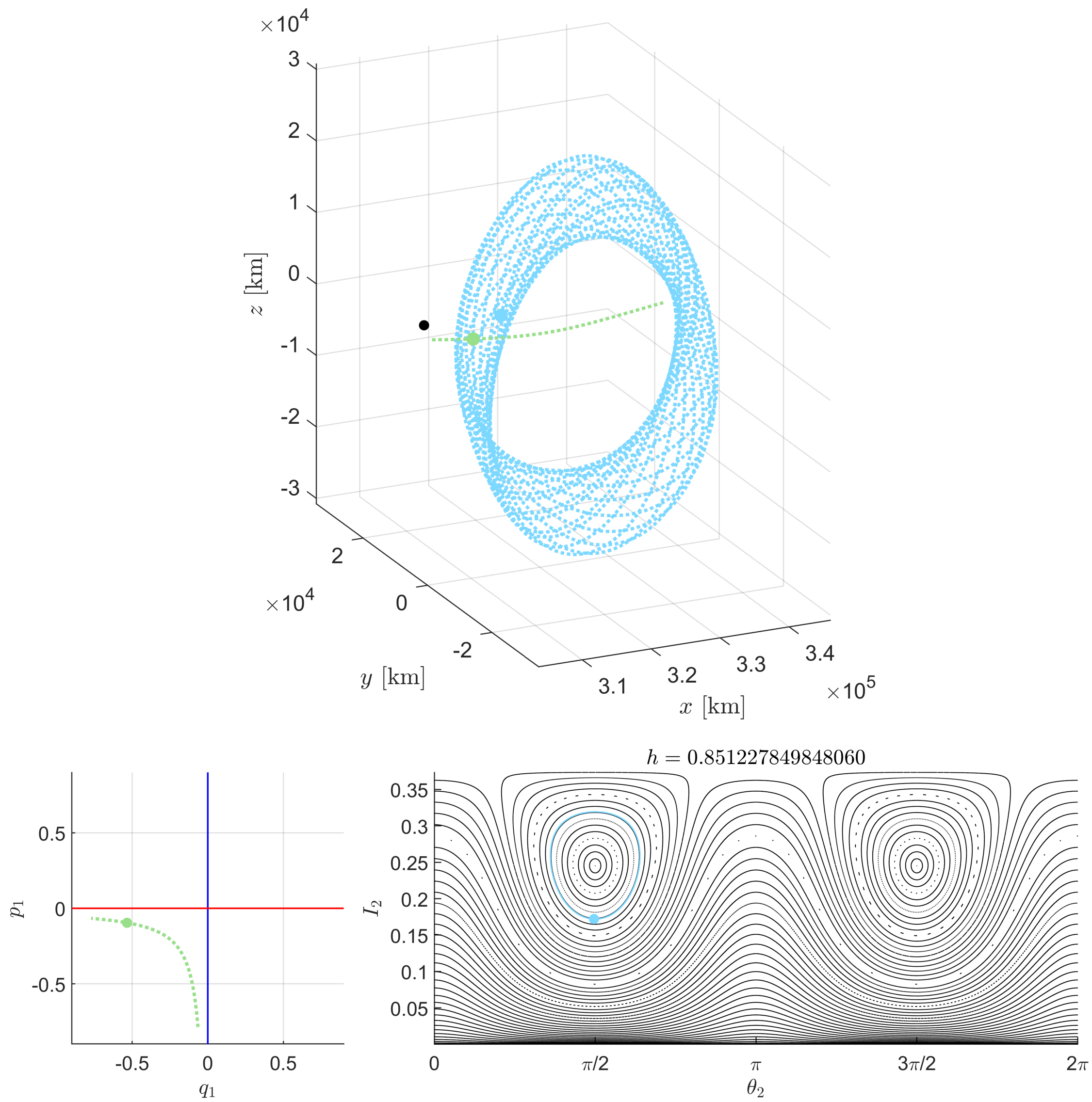

Figure 4. RLOE decomposition of a random point near EM L_1.

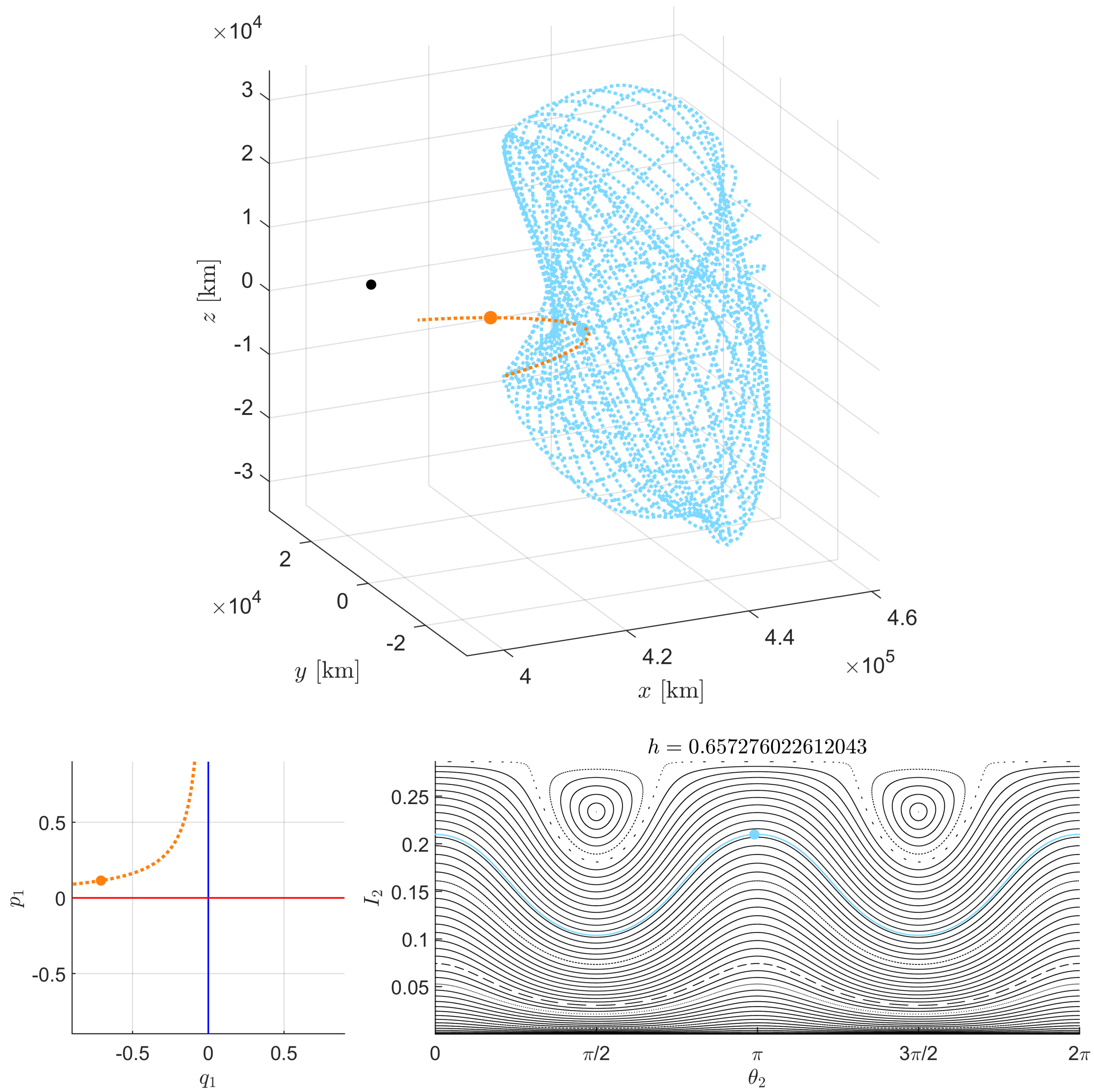

Figure 5. RLOE decomposition of a random point near EM L_2.

FLOW MAP PARAMETERIZATION METHOD

In the remainder of the paper, we illustrate the utility of the RLOE Strategic Visualization Tool using a controlled trajectory as an example. The control strategy employed, the Floquet mode approach, has a similar intuition to the LOE/RLOE control strategy previously developed,[4,9] and is elaborated upon for 2-dimensional quasi-periodic orbits in the following section. The nominal trajectory chosen is an L_1 quasi-halo orbit. As we shall see in the following section, the implementation of the Floquet mode approach for quasi-periodic orbits can be greatly simplified by using the Flow Map Parameterization method[17,19] (FMP) to compute the nominal trajectory. Hence, we devote the present section for background on FMP. The main attribute of FMP useful for Floquet mode approach is the so-called adapted frame that gives us a similar basis to the Floquet modes.

Invariance Equations

Invariant Tori Let ϕ_t be the flow of the CR3BP generated by the Hamiltonian in Equation 1. To compute a 2-dimensional quasi-periodic libration point orbit in the CR3BP is to look for a parameterization $\hat{K} : \mathbb{T}^2 \to \mathbb{R}^6$ of a 2-dimensional torus $\hat{\mathcal{K}} \subset \mathbb{R}^6$ invariant under CR3BP dynamics. To save computational time and complexity, one may look instead for a parameterization $K : \mathbb{T}^1 \to \mathbb{R}^6$ of a 1-dimensional torus (i.e., a curve) $\mathcal{K} \subset \hat{\mathcal{K}}$, invariant under a time-T map, where T is the period associated to one of the internal frequencies of $\hat{\mathcal{K}}$ (often called the stroboscopic time). Under the time-T map (called the "flow map"), the invariance equation for K is:

$$\phi_T(K(\theta)) - K(\theta + \rho) = 0, \tag{19}$$

where ρ is the rotation number of the invariant curve K.

Invariant Bundles We consider here 2-dimensional quasi-periodic orbits that are partially hyperbolic, as they are sufficiently close to the libration point. Hence, these tori have invariant bundles of rank 1, namely, the linear stable/unstable directions. Exploiting the flow map, we look for a parameterization $W : \mathbb{T}^1 \to \mathbb{R}^6$ of a bundle $\mathcal{W}$ with base $\mathcal{K}$ satisfying the invariance equation:

$$\mathrm{D}_z\phi_T(K(\theta))W(\theta) = W(\theta + \rho)\lambda, \tag{20}$$

where $\lambda = e^{T\chi}$ for $\chi \in \mathbb{R}$, and where z in this context refers to $z = (q, p) \in \mathbb{R}^6$, not to be confused with the vertical synodic coordinate in the CR3BP. From $\mathcal{W}$ we can recover the bundle $\hat{\mathcal{W}}$ of $\hat{\mathcal{K}}$, just as we can recover the torus $\hat{\mathcal{K}}$ from the invariant curve $\mathcal{K}$. If $\chi < 0$ (i.e., $\lambda < 1$), $\hat{\mathcal{W}} = \hat{\mathcal{W}}^s$ is the stable bundle and if $\chi > 0$ (i.e., $\lambda > 1$), $\hat{\mathcal{W}} = \hat{\mathcal{W}}^u$ is the unstable bundle.

Adapted Frames

The key feature of FMP we utilize for Floquet mode control is the computation of an adapted frame for the torus. An adapted frame is a suitable symplectic change of coordinates for each point on the torus so that its linear dynamics reduce to an upper triangular matrix:

$$\hat{P}(\theta + \rho)^{-1}\mathrm{D}_z\phi_T(K(\theta))\hat{P}(\theta) = \left(\begin{array}{c|c} \Lambda & S(\theta) \\ \hline O_n & \Lambda^{-\mathsf{T}} \end{array}\right), \tag{21}$$

with

$$\Lambda = \begin{pmatrix} I_2 & 0 \\ 0 & \lambda \end{pmatrix}, \quad S(\theta) = \begin{pmatrix} S_1(\theta) & 0 \\ 0 & 0 \end{pmatrix}, \tag{22}$$

where each 0 block corresponds to a zero matrix of suitable dimensions and $S_1(\theta)$ is the 2×2 symmetric matrix called the torsion matrix.[17,19]

The adapted frame $P(\theta)$ is constructed out of two subframes: $P(\theta) = \begin{pmatrix} L(\theta) & | & N(\theta) \end{pmatrix}$. The subframe $L(\theta)$ is required to satisfy:

$$\mathrm{D}_z\phi_T(K(\theta))L(\theta) = L(\theta + \rho)\Lambda. \tag{23}$$

Observing that $\mathrm{D}_\theta K$, W, and the CR3BP vector field X_H are invariant under the differential of time-T maps, the subframe $L : \mathbb{T}^1 \to \mathbb{R}^{6\times 3}$ is given by:

$$L(\theta) := \begin{pmatrix} \mathrm{D}_\theta K(\theta) & X_H(\theta) & W(\theta) \end{pmatrix}. \tag{24}$$

Assuming a standard Euclidean metric, we can construct a suitable complementary subframe as

$$\hat{N}(\theta) = \Omega L(\theta)(L(\theta)^\top L(\theta))^{-1}. \tag{25}$$

This choice of frame reduces the linear dynamics to the desired form in Equation 21, but we can transform the normal bundle to further reduce the linear dynamics such that $S(\theta)$ takes the constant form:

$$S(\theta) = \begin{pmatrix} S & 0 \\ 0 & 0 \end{pmatrix}. \tag{26}$$

where S_1 is a 2×2 symmetric matrix called the torsion.[17,19] We can find a transformation of the following form

$$P(\theta) = \hat{P}(\theta) \begin{pmatrix} I & B(\theta) \\ 0 & I \end{pmatrix}, \tag{27}$$

where $B(\theta)$ rotates the normal bundle to remove periodic components of the normal frame and can be computed from the cohomological equations

$$\Lambda B(\theta) - B(\theta + \rho)\Lambda^{-1} = S(\theta) - \langle S(\theta) \rangle, \tag{28}$$

which can be solved component-wise using the solutions discussed in the next section. We direct readers to Haro et al.[17,19] for more details.

Relation to Periodic Orbits The adapted frame computed in FMP is similar to the eigenbasis decomposition of a periodic orbit. Suppose $z_0 = (q_0, p_0)$ is the fixed point of the flow map. In suitable coordinates, given by a symplectic change of coordinates P, the linear dynamics given by the monodromy matrix $A \coloneqq \Phi(T) = \mathrm{D}_z\phi_T(z_0)$ reduce to a block diagonal matrix:

$$P^{-1}\mathrm{D}_z\phi_T(z_0)P = D, \quad D = \mathrm{diag}(D_1, D_2, D_3), \tag{29}$$

where

$$D_1 = \begin{pmatrix} \lambda & 0 \\ 0 & \lambda^{-1} \end{pmatrix}, \quad D_2 = \begin{pmatrix} 1 & \epsilon \\ 0 & 1 \end{pmatrix}, \quad D_3 = \begin{pmatrix} \cos\alpha & -\sin\alpha \\ \sin\alpha & \cos\alpha \end{pmatrix}. \tag{30}$$

Thus, the adapted frame P is a generalization of the eigenbasis commonly used in astrodynamics for periodic orbits to quasi-periodic orbits. As the Floquet modes are built with the columns of P in the periodic orbit case, so too will they be constructed out of the columns of $P(\theta)$ in the quasi-periodic orbit case of Floquet mode control discussed in the next section.

Description of a Newton Step

One of the primary computational benefits of FMP over other torus computation algorithms is the speedup from $\mathcal{O}(N^3)$ to $\mathcal{O}(N \log N)$ in time compared to similar algorithms.[17] Such a speedup is made possible by exploiting the symplectic geometry of the problem (via the adapted frame) so that each iteration in the Newton step is accomplished by explicitly solving so-called cohomological equations, rather than by inverting large matrices. When computing objects related to the torus, we often represent them as Fourier series. For example, for some function $\xi : \mathbb{T}^1 \to \mathbb{R}$ that is 1-periodic in θ, we consider the Fourier series of ξ as:

$$\xi(\theta) = \sum_{k \in \mathbb{Z}} \hat{\xi}_k e^{i2\pi k\theta}, \tag{31}$$

where $i = \sqrt{-1}$. The average is simply the zero term:

$$\hat{\xi}_0 = \langle \xi \rangle \coloneqq \int_{\mathbb{T}^1} \xi(\theta)\mathrm{d}\theta. \tag{32}$$

Cohomological Equations There are two kinds of cohomological equations encountered here: non-small divisors and small divisors. Let us first consider the case of non-small divisors. Let $\xi, \eta : \mathbb{T}^1 \to \mathbb{R}$ be analytic functions represented as Fourier series. The non-small divisors cohomological equations are functional equations of the form:

$$c_1\xi(\theta) - c_2\xi(\theta + \rho) = \eta(\theta), \tag{33}$$

where $c_1, c_2 \in \mathbb{R}$ such that $|c_1| \neq |c_2|$, where ρ is the rotation number, and where η and ρ are known and ξ is to be found. In other words, we solve for the Fourier coefficients of ξ by:

$$\hat{\xi}_k = \frac{\hat{\eta}_k}{c_1 - c_2 e^{i2\pi k\rho}} \quad \forall k. \tag{34}$$

The case of small divisors is the case where the functional equation takes the form:

$$\xi(\theta) - \xi(\theta + \rho) = \eta(\theta), \tag{35}$$

where η and ρ are known and ξ is to be found. If $\langle \eta \rangle = 0$, the solution is then given by:

$$\hat{\xi}_0 \in \mathbb{R} \quad \text{free}, \qquad \hat{\xi}_k = \frac{\hat{\eta}_k}{1 - e^{i2\pi k\rho}} \quad \forall k \neq 0. \tag{36}$$

Newton step on the torus Given (K, W, λ) that approximately satisfy Equations 19 and 20, we perform an iterative Newton scheme to improve the accuracy of the approximation. For the Newton step on the torus, we define the error as a function $E^K : \mathbb{T}^1 \to \mathbb{R}^6$ given by:

$$E^K(\theta) \coloneqq \phi_T(K(\theta)) - K(\theta + \rho). \tag{37}$$

We compute the correction $\Delta K : \mathbb{T}^1 \to \mathbb{R}^6$ to the parameterization K, leading to the updated invariance equation:

$$\phi_T(K(\theta) + \Delta K) - K(\theta + \rho) - \Delta K(\theta + \rho) = 0. \tag{38}$$

Following Fernández-Mora et al.,[19] we linearize the equation around the approximate torus to find the correction ΔK that makes satisfies the invariance equation at first order. We use the adapted frame P to write the correction in coordinates so that $\Delta K(\theta) = P(\theta)\xi(\theta)$. Expanding around the approximated torus and ignoring higher-order terms gives:

$$\mathrm{D}_z\phi_T(K(\theta))P(\theta)\xi(\theta) - P(\theta + \rho)\xi(\theta + \rho) = -E^K(\theta). \tag{39}$$

The update ΔK can then be solved as a sequence of cohomological equations.[17,19]

Newton step on the bundle For the Newton step on the bundle, we define the error as a function $E^W : \mathbb{T}^1 \to \mathbb{R}^6$ given by:

$$E^W(\theta) \coloneqq \mathrm{D}_z\phi_T(K(\theta))W(\theta) - W(\theta + \rho)\lambda. \tag{40}$$

Following a similar strategy as the Newton step on the torus, we look for corrections to the bundle and Floquet multiplier $\Delta W : \mathbb{T}^1 \to \mathbb{R}^6$ and $\Delta\lambda \in \mathbb{R}$, respectively. The invariance equation is then:

$$\mathrm{D}_z\phi_T(K(\theta))(W(\theta) + \Delta W(\theta)) - (W(\theta + \rho) + \Delta W(\theta + \rho))(\lambda + \Delta\lambda) = 0. \tag{41}$$

Similarly, we choose corrections to solve the updated invariance equation at first order, writing the correction term for the bundle in coordinates so that $\Delta W(\theta) = P(\theta)\xi(\theta)$. Expanding the updated invariance equation to first order gives:

$$\mathrm{D}_z\phi_T(K(\theta))P(\theta)\xi(\theta) - P(\theta + \rho)\xi(\theta + \rho)\lambda - W(\theta + \rho)\Delta\lambda = -E^W(\theta). \tag{42}$$

The updates ΔW and $\Delta\lambda$ can then be solved as a sequence of cohomological equations.[17,19]

Results

Figure 6 shows a Northern quasi-halo orbit around EM L_1 computed using the flow map parameterization method, with a z-amplitude of about 40,000 km. This orbit was chosen to be a quasi-halo around L_1 sufficiently close to the libration point so that a posteriori analysis is possible via RLOE methods. In particular, this orbit can be used as a candidate for a posteriori analysis via the RLOE Strategic Visualization Tool, as well as for the Floquet mode approach for stationkeeping quasi-periodic orbits described in the following section.

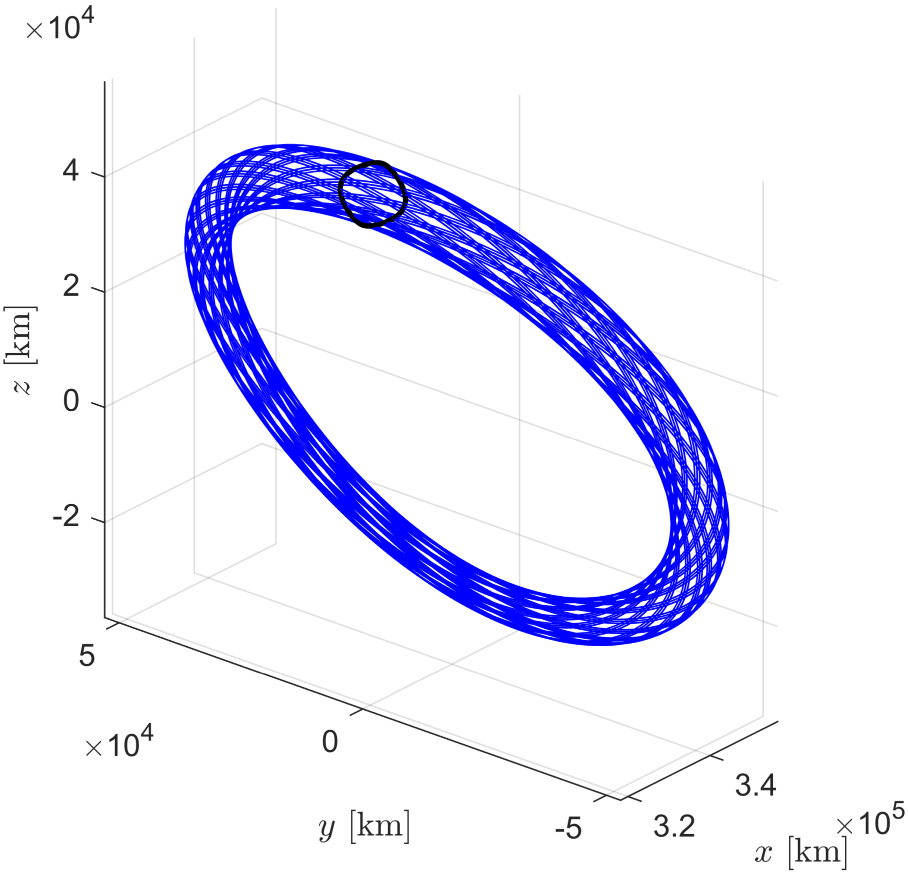

Figure 6. EM L_1 Northern quasi-halo computed using the Flow Map Parameterzation method.

STATIONKEEPING: THEORY, SIMULATION, ANALYSIS

In space mission design, it is useful and necessary to consider stationkeeping approaches so that a spacecraft can maintain a desired orbit under additional perturbations or errors not modeled by the simplified dynamical model, i.e., the CR3BP. As described in Peterson et al.[4] and later investigated by Hunsberger et al.,[9] one approach is to nullify the unstable coordinate, q_1, in LOEs or RLOEs. The limitation of this and similar normal form approaches is that one must map the spacecraft state near the Lagrange point into the simplified dynamical system, designing maneuvers therein; hence, the approximation made by the simplified system is the limiting factor in the method's feasibility. Moreover, the primary utility of the LOE approach–simplicity–may be lost when designing stationkeeping maneuvers in this way. A more practical strategy is one that can readily generalize to increasingly realistic models, rather than relying on an even more simplified one. Fortunately, the core principle of these normal form stationkeeping approaches–nullifying the projection onto the unstable manifold–persists in a methodology called the Floquet Mode Approach (FMA).[10,11,13,15]

Theory: Floquet Mode Approach for Periodic Orbits

Originally developed by Wiesel and Shelton[10] for stationkeeping a periodic orbit near EM L_3 perturbed by the Sun, FMA utilizes the eigenspace decomposition of the monodromy matrix of an orbit, M, that is, the state transition matrix over one period. The Floquet mode approach is detailed in Chapter 3 of the first volume of the books by Gómez et al.[12] We reproduce some of the theory for periodic orbits for the sake of completeness, as the generalization to quasi-periodic orbits will be a straightforward extension. Consider, as Gómez et al., a periodic orbit in the CR3BP of stability type saddle $\times$ center. The monodromy matrix of the periodic orbit, $A = \Phi(T) = \mathrm{D}_z\phi_T(z_0)$, has 6 eigenvalues: $\lambda_1 > 1$, $\lambda_2 = \lambda_1^{-1} < 1$, $\lambda_3 = \lambda_4 = 1$, and $\lambda_5 = \overline{\lambda}_6$ complex of modulus 1. Denote the corresponding eigenvectors by $e_i(0)$ for $i = 1, \ldots, 6$. Now, the adapted frame for the periodic orbit, P, puts the monodromy matrix, A, into the block diagonal form in Equation 29. In the case of periodic orbits, this adapted frame is constructed by putting the eigenvectors as its columns:

$$P = \begin{pmatrix} | & & | \\ e_1(0) & \cdots & e_6(0) \\ | & & | \end{pmatrix}. \tag{43}$$

Using this adapted frame, the monodromy matrix takes the block diagonal form (as in Equation 29):

$$P^{-1} D_z\phi_T(z_0) P = \begin{pmatrix} \lambda_1 & 0 & & & & \\ 0 & \lambda_1^{-1} & & & & \\ & & 1 & \epsilon & & \\ & & 0 & 1 & & \\ & & & & \cos\alpha & -\sin\alpha \\ & & & & \sin\alpha & \cos\alpha \end{pmatrix}, \tag{44}$$

where, if r is the real part of λ_5, then $\alpha = \arccos r - 2\pi$. With this matrix in mind, we define the Floquet modes. In short, they are related to the eigenvectors that span P. The Floquet modes, denoted by $\overline{e}_i(t)$, $i = 1, \ldots, 6$, are T-periodic vectors that we can write in terms of the $e_i(t)$. Note that the time dependency of the $e_i(t)$ comes from shifting along the underlying periodic orbit; these can be obtained from the variational equations, for example, $e_1(t) = A(t)e_1(0)$.

The first two Floquet modes are defined as:

$$\overline{e}_i(t) = e_i(t)\exp\left(-t\frac{\ln\lambda_i}{T}\right), \quad i = 1, 2, \tag{45}$$

where T is the orbit period. The third Floquet mode is the tangent vector to the orbit, which is already a periodic function: $\overline{e}_3(t) = e_3(t)$. The fourth mode is decomposed as:

$$\overline{e}_4(t) = e_4(t) - \epsilon(t)e_3(t), \tag{46}$$

where $\epsilon(t) = \frac{t}{T}\epsilon(0)$ and $\epsilon(0)$ appears in Equation 44. Finally, if $e_5(0) + ie_6(0)$ is the complex eigenvector related to λ_5, and $e_5(t) + ie_6(t) = A(t)(e_5(0) + ie_6(0))$, then the remaining two

Floquet modes are defined as:

$$\overline{e}_5(t) = \cos\left(-\frac{\alpha t}{T}\right) e_3(t) - \sin\left(-\frac{\alpha t}{T}\right) e_4(t), \tag{47}$$

$$\overline{e}_6(t) = \sin\left(-\frac{\alpha t}{T}\right) e_3(t) + \cos\left(-\frac{\alpha t}{T}\right) e_4(t). \tag{48}$$

With the Floquet modes computed, we follow Farres et al.[15] in their succinct description of the control strategy. Let $\delta = (\delta x, \delta y, \delta z, \delta\dot{x}, \delta\dot{y}, \delta\dot{z})^\top$ be a deviation vector between the spacecraft state (e.g., computed from tracking data) and the nominal point on the nominal orbit. At some time t, we write the deviation in the local basis $\{\overline{e}_i(t)\}$ defined by the Floquet modes:

$$\delta = \sum_{i=1}^{6} c_i \overline{e}_i(t). \tag{49}$$

In the Floquet Mode Approach strategy, we seek to perform a maneuver that cancels the component c_1, as $\overline{e}_1(t)$ is the unstable Floquet mode. Using a projection operator, $\pi^1(t)$, we can write:

$$c_1 = \langle \pi^1(t), \delta(t) \rangle, \qquad \text{where } \pi^1(t) = \frac{\overline{e}_1(t)}{\|\overline{e}_1(t)\|}. \tag{50}$$

Denoting by $\Delta = (0, 0, 0, \Delta v_x, \Delta v_y, \Delta v_z)^\top$ the maneuver to cancel the unstable component, c_1, of δ, we obtain:

$$\delta + \Delta = (\delta x, \delta y, \delta z, \delta\dot{x} + \Delta v_x, \delta\dot{y} + \Delta v_y, \delta\dot{z} + \Delta v_z)^\top \tag{51}$$

$$= \sum_{i=2}^{6} c_i \overline{e}_i(t). \tag{52}$$

Thus, the above equalities imply $\langle \pi^1(t), \Delta \rangle = -c_1$; hence, the manuever must satisfy:

$$\pi^1_4(t)\Delta v_x + \pi^1_5(t)\Delta v_y + \pi^1_6(t)\Delta v_z = -c_1. \tag{53}$$

Following Farres et al.,[15] we take the minimum norm solution given by:

$$(\Delta v_x, \Delta v_y, \Delta v_z) = \left(\frac{-c_1\pi^1_4(t)}{\beta(t)}, \frac{-c_1\pi^1_5(t)}{\beta(t)}, \frac{-c_1\pi^1_6(t)}{\beta(t)}\right). \tag{54}$$

where $\beta(t) = \sqrt{\pi^1_4(t)^2 + \pi^1_5(t)^2 + \pi^1_6(t)^2}$.

Theory: Floquet Mode Approach for Quasi-periodic Orbits

One of the primary goals in preliminary mission design is to produce valid trajectories over long periods of time in the most realistic system possible, often an ephemeris model. So, stationkeeping strategies that are generalizable to higher-fidelity models are typically preferred over model-restricted approaches. The philosophy of FMA is simple to state–remove a trajectory's instability when it becomes too large–but this process is not yet possible in an ephemeris model. As we increase the fidelity of the model from the CR3BP into intermediate periodically and quasi-periodically forced models, quasi-periodic orbits become the primary orbit option–even the 9:2

NRHO becomes a quasi-periodic orbit in some intermediate models. So, generalizing the Floquet mode approach for stationkeeping to quasi-periodic orbits is one step toward the goal of a simple, logical, and generalizable stationkeeping procedure.

The modifications required for quasi-periodic orbits are only in the definition of the Floquet modes themselves. The remaining control theory is identical to the periodic orbit case. As we compute quasi-periodic orbits in this work using the Flow Map Parameterization method, a method which relies on the underlying system being Hamiltonian, using canonical position-momentum (q, p) variables, we note that an instantaneous ΔV with fixed position results in an instantaneous change in momentum Δp and vice versa. Hence, we proceed by generalizing the description of the Floquet modes for quasi-periodic orbits computed via Flow Map Parameterization method.

Given an adapted frame $P(\theta)$ that puts the matrix $\mathrm{D}_z\phi_T(K(\theta))$ into the following form, as in Equation 21:

$$P(\theta+\rho)^{-1}\mathrm{D}_z\phi_T(K(\theta))P(\theta) = \left(\begin{array}{c|c} \Lambda & S \\ \hline O_n & \Lambda^{-\mathsf{T}} \end{array}\right), \tag{55}$$

with

$$\Lambda = \begin{pmatrix} I_2 & 0 \\ 0 & \lambda \end{pmatrix}, \quad S = \begin{pmatrix} S_1 & 0 \\ 0 & 0 \end{pmatrix}, \tag{56}$$

where each 0 block corresponds to a zero matrix of suitable dimensions and S_1 is the 2×2 symmetric matrix called the torsion matrix.[17,19] With the matrix on the right-hand side of Equation 55 in mind, we construct the Floquet modes for the quasi-periodic invariant torus. Denote the columns of $P(\theta)$ by $e_i(\theta, 0)$ for $i = 1, \ldots, 6$. Note that the e_i depend on an angle θ along the invariant curve of the flow map, as well as a time $t \in [0, T]$ along the flow, i.e., away from the stroboscopic section. Finally, observe that the adapted frame can additionally be defined around the entire invariant torus: $P(\theta, t)$. Then, the adapted frame at intermediate times is given by: $P(\theta, t) = \Phi(t)P(\theta, 0)$.

The first two Floquet modes here are defined by:

$$\overline{e}_i(\theta, t) = e_i(\theta, t), \quad i = 1, 2. \tag{57}$$

The conjugate modes, $\overline{e}_{4,5}(\theta, t) \in \mathbb{R}^{6\times2}$, are modified by the elements of the torsion matrix, S_1, similar to the fourth Floquet mode in the periodic orbit case:

$$\overline{e}_{4,5}(\theta, t) = e_{4,5}(\theta, t) - e_{1,2}(\theta, t)V(\theta, t), \tag{58}$$

where

$$V(\theta, t) = \frac{t}{T}S_1 + B_1(\theta) - B_1(\theta + \omega t). \tag{59}$$

Finally, the stable and unstable Floquet modes are defined as in the periodic orbit case:

$$\overline{e}_3(\theta, t) = e_3(\theta, t) \exp\left(-t\frac{\ln\lambda}{T}\right), \tag{60}$$

$$\overline{e}_6(\theta, t) = e_6(\theta, t) \exp\left(+t\frac{\ln\lambda}{T}\right), \tag{61}$$

where $\lambda < 1$ is the stable eigenvalue, and where we use properties of the logarithm to simplify the second expression, i.e., $\ln\lambda^{-1} = -\ln\lambda$.

The remaining procedure follows similarly tothe periodic orbit case, with some choice over projection onto the nominal invariant curve at time t. First, project the deviation into the Floquet mode basis at time t. Note that we perform the change of variables to put the Floquet mode basis at time t into position-velocity coordinates. Next, project the deviation onto the unstable Floquet mode–here we would switch π^1 to π^6 using the notation of this section. Then, we compute the maneuver Δ in the same way, applying as an instantaneous change in velocity the stationkeeping maneuver.

Remarks on Higher-fidelity Models The goal of developing Floquet mode approach for quasi-periodic orbits is to ultimately generalize to higher-fidelity intermediate models such as the periodically forced models–Elliptic R3BP, Hill R4BP (HR4BP), or (Quasi-)Bicircular R4BP–or quasi-periodically forced models–Inclined HR4BP, Eccentric HR4BP, or IE-HR4BP. So, how does the Floquet mode approach generalize for quasi-periodic orbits in (quasi-)periodically forced models? The setup is similar but depends on the dimension of the torus and its linear normal behavior, i.e., its stability. In any case, if the Flow Map Parameterization method is used for the computation of the quasi-periodic orbit, the flow map can be exploited in an identical way to produce the Floquet modes. If the orbit has an elliptic part, then the Floquet modes corresponding to those directions will be defined as a rotation as in Equation 47. If there are multiple hyperbolic modes, then the control strategy may change; however, if one of the unstable eigenvalues dominates the other(s), then the same strategy will work, as that direction dominates the instability.

Proposed Simulation

To understand the effect of the RLOE visualization tool on a trajectory around a Lagrange point in cislunar space, possibly identifying differences in the normal form and Floquet mode representations, we propose a stationkeeping simulation around the Northern L_1 quasi-halo orbit with 40,000 km of z amplitude computed in the previous section, shown in Figure 6, as the reference orbit. For a given state of the satellite $\tilde{\gamma}(t)$ at a certain epoch t, we define an associated nominal point as the point of the nominal orbit $\gamma(t)$ isochronous with the spacecraft, following Farres et al.[15] For the quasi-halo orbit, we use the isochronous point as well as the point on the initial invariant curve having $\theta = 0$. However, the nominal point $\theta = 0$ will require an update at each maneuver time, due to the drift along the invariant curve, as we have observed in preliminary calculations.

We propose to run this simulation, propagating the reference orbit for 5 stroboscopic periods, applying routine stationkeeping maneuvers using the Floquet mode approach for quasi-periodic orbits developed in the previous section. The displaced initial condition will be generated by introducing a random error in the spacecraft state of 5×10^{-5} in dimensionless units, corresponding to approximately 20 km error in position and 5 cm/s error in velocity. In the simulation, routine stationkeeping maneuvers will be performed each time the perturbed trajectory is at a distance of 1×10^{-4} DU (≈ 40 km) along the unstable direction from the nominal point on the quasi-halo orbit. Additionally, we will apply a 5% error in the modulus of the maneuver for each maneuver.

Remarks on RLOE Analysis The result of the proposed stationkeeping simulation will be a controlled trajectory that remains close to the nominal quasi-halo orbit through successive maneuvers that eliminate the deviation in the unstable component of the nominal orbit. As the satellite remains sufficiently close to the nominal orbit due to our tolerances, the local first-order approximation by the Floquet modes suffices. In reality, when a maneuver is performed, the energy of the satellite is modified, and the underlying quasi-periodic orbit "closest" to the satellite changes. Using the RLOE Strategic Visualization Tool allows one to see the underlying quasi-periodic orbit that is "closest" to the satellite following successive stationkeeping maneuvers. One can stack multiple Poincaré sections of the center manifold as a Thick-Poincaré section, as in Jorba et al.,[20] or, alternatively, one can consider visualizing the underlying quasi-periodic orbits in the Poincaré map adding a third dimension for the change in energy following the resulting sequence of maneuvers.

While we do not expect to see this orbit change significantly, the tool remains useful if a transfer or formation must be designed to/from or around the new orbit. For example, the accuracy for follow-on missions improves as the new nominal orbit is uncovered via RLOEs. Moreover, the stable/unstable Floquet modes and RLOEs (q_1, p_1) approximate the same instability of the quasi-halo orbit in different ways. On the one hand, the Floquet modes are generated from the linear approximation of the dynamics around the particular quasi-halo orbit; on the other hand, the RLOEs are generated from a higher-order normal form approximation of the dynamics around the Lagrange point L_1. Thus, we will compare the resulting projection onto the unstable Floquet mode with the unstable manifold coordinate of the RLOEs, i.e., q_1. If they are within a desired tolerance, then, for the purposes of the simulation, the RLOEs qualitatively characterize the behavior in substantial region around L_1 (and similarly for an experiment around L_2).

CONCLUDING REMARKS

In this paper, we presented the inclusion of halo and quasi-halo orbits into the local orbital element framework by constructing so-called resonant local orbital elements (RLOEs) using a 1:1 resonant normal form. By keeping those terms in the Hamiltonian expansion corresponding to the 1:1 resonance in the center manifold, halo and quasi-halo orbits were retained at the expense of one first integral. The system losing its explicit integrability adds an extra step to orbit generation; however, by computing a Poincaré map in RLOEs, we showed that periodic Lyapunov and halo orbits, as well as quasi-periodic Lissajous and quasi-halo orbits, can be readily parameterized and generated from the Poincaré map. Using the RLOEs, we introduced a Strategic Visualization Tool that is a vector space decomposition of the dynamics around $L_{1,2}$, splitting an arbitrary point around a Lagrange point into distinct saddle and center projections. The Strategic Visualization Tool allows one to identify an arbitrary spacecraft state and assign to it a particularly periodic or quasi-periodic orbit that is "closest" in the center projection, as well as a saddle trajectory "closest" in the saddle projection. The RLOE Strategic Visualization Tool simplifies the dynamics around $L_{1,2}$ by separating states into their fundamental dynamic modes.

As an application of the RLOE Strategic Visualization Tool, we proposed the use of a controlled trajectory around L_1. Using the flow map parameterization method, we computed a Northern L_1 quasi-halo orbit and derived the Floquet modes for a quasi-periodic orbit used in the Floquet mode approach for stationkeeping in the CR3BP. The Floquet mode approach is a stationkeeping strategy that nullifies the unstable component of the perturbed trajectory. The flow map parameterization method enables a simple generalization of the Floquet mode approach for quasi-periodic orbits that can be further applied to quasi-periodic orbits in (quasi-)periodically forced models of the Earth-Moon system. The RLOE Strategic Visualization Tool was then proposed to be used for a posteriori analysis of the stationkeeping method. In particular, we conjecture that the stationkeeping maneuver that nulls the instability in the Floquet basis will similarly, though not exactly, null the unstable manifold coordinate of the RLOEs, i.e., q_1. Furthermore, the Strategic Visualization Tool provides quick insight into the change in the underlying orbit, ultimately improving the accuracy of the new nominal orbit for follow-on missions. Future work includes successfully implementing the stationkeeping simulation, performing examples to include orbits around L_2, as well as using the RLOE Strategic Visualization Tool to compare with additional stationkeeping approaches.

ACKNOWLEDGMENTS

The authors dedicate this work to the late Professor Àngel Jorba, and thank him for his contributions to our field, years of mentorship, and a lifetime of inspiration. This work has been approved for public release; distribution is unlimited. Public Affairs release approval AFRL-2025-3585. The views expressed are those of the authors and do not reflect the official guidance or position of the United States Government, the Department of Defense or of the United States Air Force.

REFERENCES

[1] M. Smith, D. Craig, N. Herrmann, E. Mahoney, J. Krezel, N. McIntyre, and K. Goodliff, "The artemis program: An overview of nasa's activities to return humans to the moon," *2020 IEEE Aerospace Conference*, IEEE, 2020, pp. 1–10.

[2] B. P. McCarthy and K. C. Howell, "Four-body cislunar quasi-periodic orbits and their application to ballistic lunar transfer design," *Advances in Space Research*, Vol. 71, No. 1, 2023, pp. 556–584.

[3] V. Szebehely, "Modifications of the Restricted Problem," *Theory of Orbit*, pp. 556–652, Elsevier, 1967, 10.1016/B978-0-12-395732-0.50016-7.

[4] L. T. Peterson and D. J. Scheeres, "Local orbital elements for the circular restricted three-body problem," *Journal of Guidance, Control, and Dynamics*, Vol. 46, No. 12, 2023, pp. 2275–2289.

[5] A. Celletti, G. Pucacco, and D. Stella, "Lissajous and Halo orbits in the restricted three-body problem," *Journal of Nonlinear Science*, Vol. 25, 2015, pp. 343–370.

[6] G. Pucacco, "Structure of the centre manifold of the L_1,L_2 collinear libration points in the restricted three-body problem," *Celestial Mechanics and Dynamical Astronomy*, Vol. 131, Oct. 2019, p. 44, 10.1007/s10569-019-9922-4.

[7] R. I. Paez and M. Guzzo, "On the semi-analytical construction of halo orbits and halo tubes in the elliptic restricted three-body problem," *Physica D: Nonlinear Phenomena*, Vol. 439, 2022, p. 133402.

[8] L. Peterson and D. Scheeres, "Local orbital element toolkit in cislunar space," *AAS/AIAA Astrodynamics Specialist Conference*, 2024.

[9] C. Hunsberger, D. Schwab, R. Eapen, and P. Singla, "Comparing normal form representations for station-keeping near cislunar libration points," *AAS/AIAA Spaceflight Mechanics Meeting*, 2025.

[10] W. Wiesel and W. Shelton, "Modal control of an unstable periodic orbit," *Journal of the Astronautical Sciences*, 1983.

[11] C. Simó, G. Gómez, J. Llibre, and R. Martınez, "Station keeping of a quasiperiodic halo orbit using invariant manifolds," *Proceed. 2nd Internat. Symp. on spacecraft flight dynamics, Darmstadt*, Vol. 255, 1986, pp. 65–70.

[12] G. Gómez, ed., *Dynamics and mission design near libration points*. No. vol. 2-5 in World scientific monograph series in mathematics, Singapore ; River Edge, NJ: World Scientific, 2001.

[13] G. Gómez, K. C. Howell, J. Masdemont, and C. Simó, "Station-keeping strategies for translunar libration point orbits," *Advances in Astronautical Sciences*, Vol. 99, No. 2, 1998, pp. 949–967.

[14] D. Williams, K. C. Howell, and D. C. Davis, "A comparison of station-keeping strategies for halo orbits," *AAS/AIAA Astrodynamics Specialist Conference*, Vol. 231, 2023, pp. 1–20.

[15] A. Farrés, C. Gao, J. J. Masdemont, G. Gómez, D. C. Folta, and C. Webster, "Geometrical analysis of station-keeping strategies about libration point orbits," *Journal of Guidance, Control, and Dynamics*, Vol. 45, No. 6, 2022, pp. 1108–1125.

[16] Y. Zhou, M. Bando, S. Hokamoto, and P. Wu, "Orbit Maintenance for Quasi-Periodic Orbit in Earth-Moon System," *TRANSACTIONS OF THE JAPAN SOCIETY FOR AERONAUTICAL AND SPACE SCIENCES, AEROSPACE TECHNOLOGY JAPAN*, Vol. 19, No. 4, 2021, pp. 562–569.

[17] A. Haro and J.-M. Mondelo, "Flow map parameterization methods for invariant tori in Hamiltonian systems," *Communications in Nonlinear Science and Numerical Simulation*, Vol. 101, 2021, p. 105859.

[18] D. L. Richardson, "A note on a Lagrangian formulation for motion about the collinear points," *Celestial Mechanics*, Vol. 22, No. 3, 1980, pp. 231–236.

[19] A. Fernández-Mora, A. Haro, and J. M. Mondelo, "Flow Map Parameterization Methods for Invariant Tori in Quasi-Periodic Hamiltonian Systems," *SIAM Journal on Applied Dynamical Systems*, Vol. 23, No. 1, 2024, pp. 127–166, 10.1137/23M1561257.

[20] À. Jorba, B. Nicolás, and Ó. Rodríguez, "A dynamical study of Hilda asteroids in the Circular and Elliptic RTBP," *Chaos: An Interdisciplinary Journal of Nonlinear Science*, Vol. 34, No. 12, 2024.